MODELING OF PRECAST COLUMNS WITH INNOVATIVE MULTI-SPIRAL REINFORCEMENT

Petr Havlásek[1], Milan Jirásek[1] and Zdeněk Bittnar[1]

[1] Department of Mechanics, Faculty of Civil Engineering, CTU in Prague, Czech Republic

Corresponding author email: petr.havlasek@fsv.cvut.cz

Abstract

Similarly to conventional circular columns with reinforcement by a single spiral, the new concept of multi-spiral reinforcement offers superior structural performance with almost arbitrary shape of the cross-section. Compared to the conventional reinforcement layout with stirrups, a similar performance is obtained at considerably lower cost, which is due to both automation of the process and more efficient use of materials. However, the optimum reinforcement layout remains unknown and current practice relies on time demanding and costly experiments. The long-term objective of the presented research is to replace the trial-and-error experimental procedure by a sophisticated optimization employing FE analysis with advanced constitutive models for concrete. The present paper focuses on predictive capabilities of such modeling techniques.

Keywords: Passive confinement, multi-spiral reinforcement, concrete, simulation, design.

1. Introduction

The multi-spiral reinforcement for precast reinforced concrete columns was initially developed by the National Taiwan University and Ruentex Engineering & Construction Co., Ltd. Similarly to conventional circular columns with one spiral, the new concept of multi-spiral reinforcement can achieve superior structural performance with an almost arbitrary shape of the cross-section. Moreover, owing to the automation involved in the production of the reinforcement, the labor cost is reduced by 33% and the material cost by 43% (Yin et al. 2011) compared to the conventional layout with stirrups and ties. It must be noted that the production of cement and steel is associated with generation of non-negligible amount of CO_2 emissions and, for the sake of sustainability, their potential should be utilized to a maximum.

In columns with spiral reinforcement, concrete is in a multiaxial stress state originating from restraints on lateral expansion induced by the transverse reinforcement. Such passive confinement increases the strength of concrete but more importantly its ductility. This type of mechanical behavior can be realistically captured by suitable material models for concrete. The model used here is the Damage-Plastic Material Model for concrete, CDPM2, proposed by Grassl and coworkers (Grassl et al. 2013).

Nowadays, the new alternative layouts of reinforcement are investigated by an inefficient trial-and-error procedure which is both costly and time demanding. The authors are convinced that if computational modeling is extensively used, in the future a large portion of these experiments can be omitted. Moreover, the detected differences in behavior can serve for updating of the computational model and thus to improvement of its prediction capabilities.

1.1. Experiments on multi-spiral reinforcement

In the last decade, the concept of multi-spiral reinforcement and other means of increasing strength of reinforced concrete members and their ductility have been widely examined. Most of the research aimed at normal-strength concrete (around 35 MPa) and at the influence of various reinforcement layouts on the load carrying capacity and ductility either in axial compression (Kuo 2008, Liang et al.

2014, Yin et al. 2012) or in cyclic bending at constant compression (Wu et al. 2013, Ou et al. 2015, Huy 2015).

Since one of the applications is bridge piers, some of the specimens were more than 10 m high and their testing required a unique experimental facility. Probably the most promising configuration for the future is the five-spiral reinforcement layout shown in Figure 1, which combines superb structural behavior, possibility of rectangular geometry and, most importantly, very efficient fabrication utilizing automation. All the above-mentioned experimental studies conclude that strength, ductility and energy dissipation increase with increasing lateral confinement, and that at constant reinforcement ratio better results are obtained with finer spacing of the lateral reinforcement, which in turn complicates the manufacturing process.

When the high-strength concrete is not properly confined, its ductility is lost, as documented in (Wang et al. 2017). Moreover, with increasing compressive strength the design codes require a higher ratio of transverse reinforcement, which can be achieved, e.g., using the cross-spiral layout (Marvel et al. 2014).
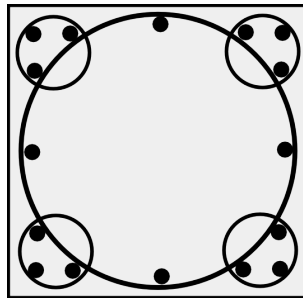
Figure 1. Innovative arrangement of reinforcement suitable for columns with square cross-section.

2. Design and modeling of concrete members with passive confinement

2.1. Design codes and recommendations

Multi-spiral reinforcement is not explicitly treated in any of the examined international standards. Usually, the design relies on formulas for a different layout of transverse reinforcement. Here we present a brief overview of the basic equations for circular members laterally and passively confined by single spiral reinforcement.

American and European standards use two distinct approaches. Despite apparent differences, both build on Richart's (1929) findings published 90 years ago. The American design procedure presented in ACI 318 (ACI 2014) defines the minimum amount of transverse reinforcement of columns, ρ_s, based on two conditions of sufficient strength and ductility.

The strength-based condition

$$\rho_s = \frac{4\,A_{st}}{s\,D_c} \geq 0.45 \frac{f'_c}{f_y}\left(\frac{A_g}{A_c} - 1\right) \tag{1}$$

guarantees that the laterally confined core of the column will be able to carry the load transferred by the concrete cover when this cover spalls off due to high axial strains. In this formula, A_{st} is the area of the spiral cross-section, s is the spiral pitch, D_c is the outer diameter of the spiral, f_c' is the specified compressive strength, f_y is the specified yield strength of reinforcement, A_g is the gross area of the cross-section and A_c is the area of concrete corresponding to D_c.

Sufficient ductility is in members loaded by a combination of compression and bending guaranteed by condition

$$\rho_s \geq 0.12 \frac{f'_c}{f_y} \tag{2}$$

Additionally, the most recent version of the US standard ACI 318-14 introduced another requirement on the reinforcement ratio in order to avoid brittle failure of high-strength concrete.

The International *fib* Model Code 2010 (fib 2012) and the new draft of the Eurocode 2 standard (EC2 2018) allow to increase concrete strength by

$$\Delta f_c = 3.5 \, \sigma_{lat}^{3/4} \, f_c^{1/4} \qquad (3)$$

as well as to increase the characteristic strains in the parabola-rectangle diagram so as to reflect the enhanced properties of confined concrete. The lateral confining stress

$$\sigma_{lat} = \frac{2 \, A_{st} f_{yd}}{s \, D_c} \qquad (4)$$

is computed simply from the equilibrium condition. Here, D_c is the spiral diameter taken to its centerline and f_{yd} is the design yield stress. In MC 2010, σ_{lat} is further reduced by a factor $1 - s/D_c$, which resembles Mander's formula (Mander et al. 1988). Opposed to this, the effective cross-sectional area where the concrete can be treated as confined is introduced only in EC 2, which adopts the idea from (Mander et al. 1988).

2.2. Prediction models

Over the past years, many prediction models for passively confined concrete have been developed. Probably the best known is the model proposed by Mander (1988) for axially confined circular concrete columns with hoops or spirals and rectangular columns with ties. This model often serves for comparison when a new model is developed. As mentioned in the previous section, certain fragments of this model have been incorporated into the design codes.

Despite a large variety of prediction models (see, e.g., a nice summary in (Kim et al. 2016)), their scope is often limited to uniaxial compression and to simple layout of reinforcement without overlap. Several promising attempts have been made to obtain the response in uniaxial compression in the case of more complex reinforcement layout. The overall response is obtained in a very simple way: the cross-section is divided into regions given by the reinforcement topology (Yin et al. 2012, Huy 2015). The stress in the overlapping zones is obtained by summing the individual contributions which correspond to the estimated lateral confinement. For instance, in the case of reinforcement layout denoted as 5S4 (1 large central spiral and 4 smaller spirals in the corners), these zones correspond to (i) unconfined concrete shell, (ii) interior of large spiral, (iii) interior of small spirals, (iv) large and small spiral overlap. However, it needs to be emphasized that in reality the stress is highly variable, especially inside the regions with highly curved spirals.

3. Numerical modeling

Even when the overall axial behavior of the members is estimated correctly with the concept outlined in the previous section, the moment and shear resistance and the bending ductility remain unknown. Therefore it is necessary to incorporate more general modelling approaches, e.g., nonlinear finite element analysis with advanced constitutive models. Recently, the response of axially compressed concrete specimens with various shapes of the cross-section wrapped by CFRP was nicely described by the microplane model (Gambarelli et al. 2014) or LDPM (Ceccato et al. 2017). The model used in the present study combines damage and plasticity and is briefly described in the following section.

3.1. Material model

The CDPM2 model, proposed in 2013 by Grassl and coworkers (Grassl et al. 2013), is an improved version of the damage-plastic model for concrete originally developed by Grassl and Jirásek (2006). The model is based on plasticity with isotropic hardening and non-associated flow (Grassl 2004), combined with a scalar damage model with damage driven by plastic flow and by the elastic strain.

The yield condition is formulated in the effective stress space and depends on all three stress invariants. The flow rule is derived from a plastic potential that depends only on the hydrostatic stress and the second deviatoric invariant. In the present study, the model is regularized by a crack-band approach (Bažant and Oh 1983) (adjustment of a parameter that controls damage propagation

depending on the finite element size). The softening curve for uniaxial tension is derived from a cohesive traction-separation law.

The model deals with the effective stress

$$\bar{\boldsymbol{\sigma}} = \mathbf{D}_e\big(\boldsymbol{\varepsilon} - \boldsymbol{\varepsilon}_p\big) \tag{5}$$

which is computed using the plastic part of the model and then reduced to the nominal stress. Here, $\boldsymbol{D}_e$ is the elastic material stiffness matrix, $\boldsymbol{\varepsilon}$ is the total strain and $\boldsymbol{\varepsilon}_p$ is the plastic strain.

The effective stress is split into the positive and negative part. The nominal stress is then evaluated as

$$\boldsymbol{\sigma} = (1 - \omega_t)\langle\boldsymbol{\sigma}\rangle^+ + (1 - \omega_c)\langle\boldsymbol{\sigma}\rangle^- \tag{6}$$

where ω_t and ω_c are two damage variables (for tension and for compression).

The model uses a large number of parameters. In (Grassl et al. 2013) it was recommended to adjust only a few basic parameters, most of which have a certain physical meaning, and to set all the other parameters to their default values. The physical parameters that can be adjusted depending on the specific type of concrete are Young's modulus, Poisson's ratio, uniaxial tensile and compression strengths, and the critical crack opening, which controls the tensile fracture energy.

3.2. Experiment and finite element model

The influence of spiral diameter, pitch and reinforcement diameter was extensively studied in (Kuo 2008), and the same experimental setup and results will be used here. All specimens had the same dimensions 600×600×1200 mm, and used 16 longitudinal rebars 25 mm. Two concrete classes with mean strengths f_{cm} = 27.7 and 34.3 MPa were used in the experiment. The experiment was focused solely on the ductility and strength under monotonous displacement-driven compression. Altogether 15 specimens were examined in the experimental study, 13 with multi-spiral 5S4 reinforcement layout shown in Figure 1 and 2 with standard hoops and ties. The vertical spacing ranged from 55 to 140 mm.

The potential of FE simulations is demonstrated on (randomly selected) specimens with multi-spiral 5S4 reinforcement (Y8, Y9) shown in Figure 1 and standard reinforcement layout with ties (R2). The only two differences between Y8 and Y9 specimens was the pitch of the spirals (75 mm for Y8 and 120 mm for Y9) and the rebar diameter of the large spiral (13 mm and 16 mm, respectively).

The mesh of the finite element model combines a structured mesh generated by an in-house mesher T3d (Rypl 2004) with irregularly discretized spiral and longitudinal reinforcement. The truss elements are linked to the volume hexahedral elements using the concept of hanging nodes. For example, in the case of Y8 model, the volume FE mesh consists of 16,000 hexahedra and the steel reinforcement mesh of 4579 truss elements. The bond between concrete and steel is treated as rigid.
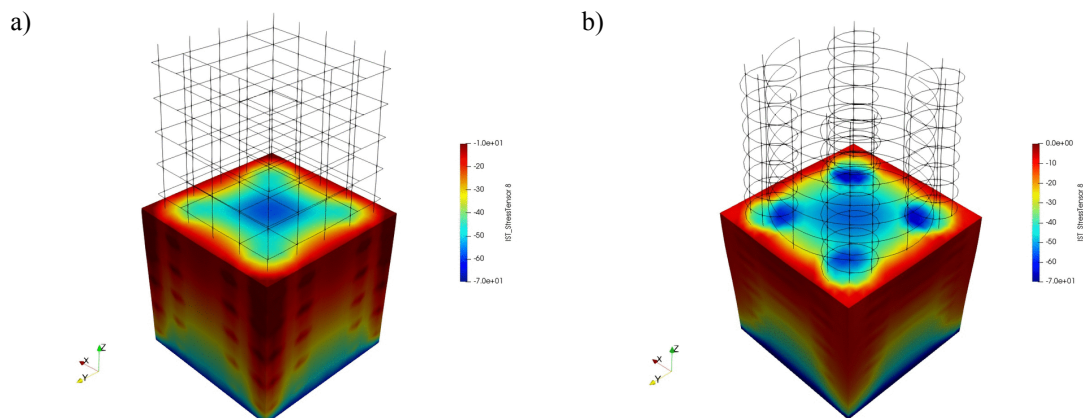
Figure 2. Distribution of vertical stress in a specimen with: a) ordinary and b) multi-spiral reinforcement.

It is assumed that the compressive and tensile strengths are in the ratio 10:1, the value of A_s is identified from simulations of compression tests under active and passive confinement. The value of the elastic modulus is derived from the compressive strength using the *fib* formula. The particular

values are f_c = 34.4 MPa, f_t = 3.44 MPa, E = 32.42 GPa, ν = 0.2, A_s = 15, w_f = 129 μm. The remaining parameters are set to their default values. The reinforcement is described by the elasto-plastic model with Mises plasticity condition, plasticity-driven hardening and damage.

The computational model is fully constrained at both ends. Free lateral expansion or an interface between the loading plates and the specimen changes the value of the ultimate strength only slightly. The analysis is run under a direct displacement control.

3.3. Results and discussion

Figure 2 shows two snapshots from postprocessing in Paraview. It compares the distribution of normal stress in the vertical direction in specimen R2 with conventional reinforcement and in Y8 with spiral reinforcement. The "concrete" is clipped in the middle of the height. The differences are remarkable. Lateral confinement, which develops in the small spirals, strengthens the concrete and enables it to bear higher stresses. Owing to the confinement, these regions have the smallest damage as illustrated in Figure 3.

The overall comparison of the computed and experimental results for the three studied geometries is shown in Figure 4a. It clearly shows that except for the peak load, which is with the present parameters of the material model slightly overestimated, the general trends are captured for the specimens with spiral reinforcement very well. A sudden drop that occurs after deformation of approximately 2% is due to the buckling of longitudinal reinforcement, which is treated as geometrically nonlinear. The biggest discrepancy is found in the case of the R2 geometry. The problem is that the experimentally determined carrying capacity does not even reach the value of the uniaxial compressive strength of concrete corrected by the contribution of the longitudinal reinforcement, as shown in Figure 4a. With perfect bond between concrete and reinforcement, the lateral confinement develops even in the setup with stirrups, which results into a substantial and perhaps spurious increase in the carrying capacity.

a)   b)
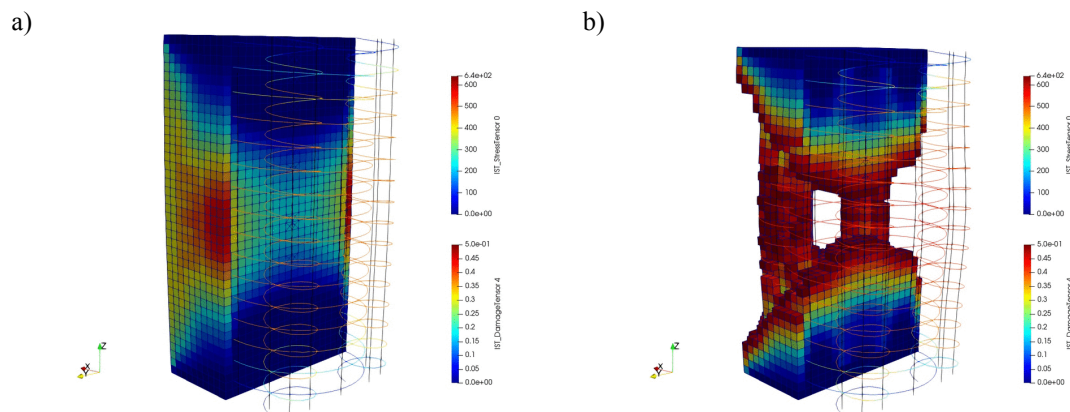
Figure 3. Distribution of compressive damage in concrete and stress in the spirals in Y8 specimen: a) at an early stage, b) after the peak; for illustration, the visibility of highly damaged elements is turned off.

The computational time of one full 3D simulation exceeded 1 day, which is unacceptable for any optimization algorithm. The computational cost can be reduced if the model covers only representative section of the model. Then, the computational time is reduced and the differences in the computed response are rather small, see (Fig. 3b). This representative section is in the present case taken equal to the pitch of the spiral. Periodic boundary conditions need to be applied at the top and bottom surfaces of such section. However, reasonable behavior is obtained even with a very coarse mesh and a model of 1/8 of the representative section. The computational time of such model slightly exceeds 10 minutes.
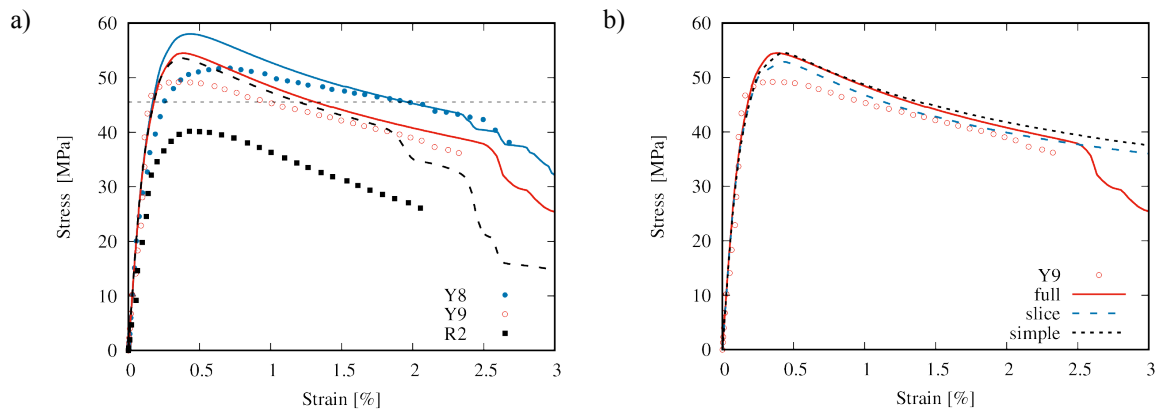
Figure 4. Comparison of a) experimental data (symbols) with the results of finite element simulations (lines), the dashed horizontal line indicates the nominal strength of concrete plus the contribution of the longitudinal reinforcement b) different alternatives of the computational model with the experimental data of Y9 specimen, the solid red line denotes the complex FE model of the entire specimen, blue dashed line corresponds to the representative section (height = 1 pitch), black short-dashed line marks the simplified and fast model suitable for parameter optimization.

4. Conclusions

The Damage-Plastic Material Model for concrete failure, proposed and implemented by Grassl and co-workers (2013) into the OOFEM finite element package (Patzák 2000, Patzák 2012), has been used for modeling of axially loaded reinforced concrete members passively confined by innovative multi-spiral reinforcement. Except for the value of the peak load, the developed computational model is able to qualitatively describe the complex behavior of columns with multi-spiral reinforcement.

The computational cost can be substantially reduced by replacing the analyzed structure by a representative section. In the future, once the role of material parameters is properly identified, the tuned computational model will serve for optimization of the reinforcement layout and probably will replace costly and time-demanding experiments.

Acknowledgments

References

ACI 318-14 (2014) Building Code Requirements for Structural Concrete and Commentary. American Concrete Institute.

Bažant, Z. P. & Oh, B. H. (1983). Crack band theory for fracture of concrete. Materiaux et Construction, 16(3), pp.155-177.

Ceccato, C., Salviato, M., Pellegrino, C. & Cusatis, G. (2017). Simulation of concrete failure and fiber reinforced polymer fracture in confined columns with different cross sectional shape. International Journal of Solids and Structures, 108.

fib Bulletin 66 (2012), Model Code 2010 - Final draft, Volume 2. Fédération Internationale du Béton (fib), Lausanne, Switzerland.

Gambarelli, S., Nistico, N. & Ožbolt, J. (2014). Numerical analysis of compressed concrete columns confined with CFRP: Microplane-based approach. Composites Part B: Engineering, 67, pp. 303-312.

Grassl, P. & Jirásek, M. (2006). Damage-plastic model for concrete failure. International Journal of Solids and Structures, 43(22), pp. 7166-7196.

Grassl, P. (2004). Modelling of dilation of concrete and its effect in triaxial compression. Finite Elements in Analysis and Design - FINITE ELEM ANAL DESIGN, 40:1021-1033.

Grassl, P., Xenos, D., Nystrom, U., Rempling, R. & Gylltoft, K. (2013). CDPM2: A damage-plasticity approach to modelling the failure of concrete. International Journal of Solids and Structures, 50(24), pp. 3805-3816.

Huy, N. S. (2015). Innovative Multi-spiral Transverse Reinforcement for Reinforced Concrete Columns. National Taiwan University.

Kim, Y.-S., Kim, S.-W., Lee, J.-Y., Lee, J.-M., Kim, H.-G. & Kim, K.-H. (2016). Prediction of stress-strain behavior of spirally confined concrete considering lateral expansion. Construction and Building Materials, 102, pp. 743-761.

Kuo, M. (2008). Axial Compression Tests and Optimization Study of 5-Spiral Rectangular RC Columns, Master Thesis (in Chinese). National Chiao Tung University, Hsinchu, Taiwan.

Liang, C.-Y., Chen, C.-C., Weng, C.-C., Yin, S. Y.-L. & Wang, J.-C. (2014). Axial compressive behavior of square composite columns confined by multiple spirals. Journal of Constructional Steel Research, 103, pp. 230-240

Mander, J. B., Priestley, M. J. N. & Park, R. (1988). Theoretical stress-strain model for confined concrete. Journal of Structural Engineering, 114(8), pp. 1804-1826.

Marvel, L., Doty, N., Lindquist, W. & Hindi, R. (2014). Axial behavior of high-strength concrete confined with multiple spirals. Engineering Structures, 60, pp. 68-80.

Ou, Y.-C., Ngo, S.-H., Roh, H., Y. Yin, S., Wang, J.-C. & Wang, P.-H. (2015). Seismic performance of concrete columns with innovative seven- and eleven-spiral reinforcement. ACI Structural Journal, 112, pp. 579-592.

Patzák, B. (2000). OOFEM home page. http://www.oofem.org.

Patzák, B. (2012). OOFEM - an object-oriented simulation tool for advanced modeling of materials and structures. Acta Polytechnica, 52(6), pp. 59-66.

prEN 1992-1-1:2018, Eurocode 2: Design of concrete structures Part 1-1:General rules, rules for buildings, bridges and civil engineering structures, Final Version of PT1-draft D3.

Richart, F., Brandtzaeg, A. & Lenoi Brown, R. (1929). Failure of plain and spirally reinforced concrete in compression.

Rypl, D. (2004). T3D mesh generator. http://mech.fsv.cvut.cz/~dr/t3d.html.

Wang, W., Zhang, M., Tang, Y., Zhang, X. & Ding, X. (2017). Behaviour of high-strength concrete columns confined by spiral reinforcement under uniaxial compression. Construction and Building Materials, 154, pp. 496-503.

Wu, T.-L., Ou, Y.-C., Yen-Liang Yin, S., Wang, J.-C., Wang, P.-H. & Ngo, S.-H. (2013). Behavior of oblong and rectangular bridge columns with conventional tie and multi-spiral transverse reinforcement under combined axial and flexural loads. Journal of the Chinese Institute of Engineers, 36, pp. 980-993.

Yin, S. Y.-L., Wu, T.-L., Liu, T. C., Sheikh, S. A., & Wang, R. (2011). Interlocking spiral confinement for rectangular columns. Concrete International, 33(12).

Yin, S. Y.-L., Wang, J.-C. & Wang, P.-H. (2012). Development of multi-spiral confinements in rectangular columns for construction automation. Journal of the Chinese Institute of Engineers, 35(3), pp. 309-320.